Microelectronic Engineering 190 (2018) 1–6

Contents lists available at ScienceDirect

Microelectronic Engineering

journal homepage: www.elsevier.com/locate/mee

Research paper

Solid-state dewetting of single-crystal silicon on insulator: effect of annealing temperature and patch size

Marco Abbarchi [a], Meher Naffouti [a,b], Mario Lodari [c], Marco Salvalaglio [d], Rainer Backofen [d], Thomas Bottein [a], Axel Voigt [d,e], Thomas David [a], Jean-Benoît Claude [a], Mohammed Bouabdellaoui [a], Abdelmalek Benkouider [a], Ibtissem Fraj [b], Luc Favre [a], Antoine Ronda [a], Isabelle Berbezier [a], David Grosso [a], Monica Bollani [c,*]

[a] Aix Marseille Université CNRS Université de Toulon IM2NP UMR 7334, 13397 Marseille, France
[b] Laboratoire de Micro-optoélectronique et Nanostructures Faculté des Sciences de Monastir Université de Monastir, 5019 Monastir, Tunisia
[c] Istituto di Fotonica e Nanotecnologie Consiglio Nazionale delle Ricerche (IFN-CNR), L-NESS laboratory, via Anzani 42, 22100 Como, Italy
[d] Institute of Scientific Computing, Technische Universität Dresden, 01062 Dresden, Germany
[e] Dresden Center for Computational Materials Science (DCMS), Technische Universität Dresden, 01062 Dresden, Germany

ARTICLE INFO

Article history:
Received 13 October 2017
Received in revised form 1 December 2017
Accepted 2 January 2018
Available online 03 January 2018

Keywords:
Solid-state dewetting
Nano-patterning
Ultra-thin silicon on insulator

ABSTRACT

We address the solid state dewetting of ultra-thin and ultra-large patches of monocrystalline silicon on insulator. We show that the underlying instability of the thin Si film under annealing can be perfectly controlled to form monocrystalline, complex nanoarchitectures extending over several microns. These complex patterns are obtained guiding the dewetting fronts by etching ad-hoc patches prior to annealing. They can be reproduced over hundreds of repetitions extending over hundreds of microns. We discuss the effect of annealing temperature and patch size on the stability of the final result of dewetting showing that for simple patches (e.g. simple squares) the final outcome is stable and well reproducible at 720 °C and for ~1 μm square size. Finally, we demonstrate that introducing additional features within squared patches (e.g. a hole within a square) stabilises the dewetting dynamic providing perfectly reproducible complex nanoarchitectures of 5 μm size.

1. Introduction

In the race towards the miniaturization of photonic and electronic components, reliable fabrication methods of nanostructures play a strategic role in the reliable implementation of innovative devices. The use of silicon films on insulator (SOI) has a central position both in photonics (e.g. on-chip photonic circuits) and electronics (e.g. fully depleted SOI MOSFET) [1]. In these contexts, an important limiting factor towards the further reduction of the dimensionality of these components is the instability upon heating of ultra-thin SOI (UT-SOI, ~12 nm thick silicon on SiO_2) [2,3,4,5]. The presence of intrinsic defects in the thin silicon layer or of ad-hoc created edges (e.g. in order to define a device) are, upon annealing even well below the inherent melting temperature of the material, the starting points of mass transport in this phenomenon ruled by surface diffusion-limited kinetics of thermally-generated adatoms, known as solid-state dewetting [6].

During dewetting, under the action of surface diffusion, mass is accumulated in a thick, receding rim at the film edges (where the curvature of the film is large), which eventually becomes unstable and evolves in elongated structures (fingers). When other instabilities, such as corner instability, bulging, rim pinch-off and faceting, take place the film breaks in isolated, monocrystalline, facetted islands [7]. The intricacies of these instabilities are further modified by the presence of preferential directions for mass transport, which must be taken into account in order to explain this complex dewetting scenario [8,9]. For example, it is well known that for a (001) oriented UT-SOI the dewetting speed along the [100] in-plane direction is much larger than that in the [110] direction [10]. These dewetting fronts are thus respectively called “unstable” and “stable”. All these phenomena render de facto impossible the practical exploitation of UT-SOI for miniaturized devices.

The underlying dewetting instability, indeed, is characterized by a defined periodicity set by the initial film thickness h_0. In real systems, however, thermal fluctuation and non-idealities (such as, e.g., the non-uniformity of the film thickness) actually make dewetting a rather disordered phenomenon and, at the end of the process, the spatial organization of the islands and their size dispersion are broadly distributed around their average values. This is an additional issue limiting the applicability of dewetted silicon films for instance, for applications in photonics [11,12].

In analogy with metals [20,21,22], a viable method for enhancing the level of ordering of the dewetted Si and SiGe structures relies on prepatterning the thin film prior to annealing [13,14,15,16]. Ordered arrays of complex islands arrangements can be obtained in a very limited set of

* Corresponding author.
E-mail address: monica.bollani@ifn.cnr.it (M. Bollani).

https://doi.org/10.1016/j.mee.2018.01.002
0167-9317/

configurations and on a limited number of repetitions by guiding the receding fronts through patches etched on the UT-SOI with a focused ion beam (FIB). This FIB-based method systematically leads to the formation of isolated (disconnected) monocrystalline islands limiting the control of the self-assembly and thus its applicability to more complex architectures. The fluctuation of the number of islands formed in a patch, their size, shape and position was between 4% and 35% [11]. More importantly, when using a FIB for etching, no receding rim was shown and the islands were always formed at the film edges at the early stages of dewetting [15]. These observations claim for spurious driving forces (e.g. ions implantation and amorphization during etching, re-crystallization during annealing) complicating the simple picture of pure surface diffusion limited-kinetics [17,18,19]. Alternative approaches based on e-beam lithography for creating small patches in the UT-SOI have been employed by several groups in the last years [20,21,22]. However, all these experimental results provided puzzling results suggesting that spurious phenomena in addition to pure surface-diffusion occurs, hindering the possibility to reproduce the results that Ye and Thompson showed for metal patches [23,24,25].

Here we show that with a proper annealing temperature and a suitable choice of pattern size and shape obtained by a combination of e-beam lithography and reactive ion etching processes, a well-controlled dewetting behaviour can be obtained also in semiconductors. We show that a perfect control of complex pattern shapes can be achieved for low annealing temperature (~720 °C) and by adding additional features within 5 μm large squared patches. Here we address the case of patches with sides oriented along the crystallographic axis [110] (the stable dewetting front). The case of patches oriented along the crystallographic axis [100] (the unstable dewetting front) is not taken into account here. In fact, in this condition, the patches rapidly undergo a fingering instability resulting in small, isolated and disordered islands [26]. Our findings fill the gap between semiconductors and thin films of metals [23,24,25] which dewetting features were expected to be general but never implemented so far in UT-SOI and opens the new possibility to exploit complex Si-based nanoarchitectures in electronic and photonic devices. Although not explicitly addressed here, it is worth mentioning that our results can be precisely reproduced by theoretical simulations based on a phase field modelling [27] providing a predictive tool for further engineering the final outcome of dewetting [16].

2. Experimental methods

An ultra-thin Si-on-insulator (UT-SOI) substrate (12 nm intrinsic Si film on 25 nm SiO_2 layer on Si(001) wafer) was patterned with a series of squares (depth ~12 nm, width of the etched squares between 0.5 μm and 5 μm) aligned along the [110] direction by means of e-beam lithography (EBL) and reactive ion etching (RIE). The resist has been spin-coated on the Si substrate and then exposed to the electron beam of a converted scanning electron microscope (SEM) along the designed pattern (acceleration voltage of 30 kV). For these kinds of structures, a single layer of PMMA diluted to 2.5% and with a molecular weight of 950 k has been employed. The dose used for the structures was 300 μC/cm^2. After the exposure, PMMA was then developed in order to remove the soluble exposed parts by a solution of methyl isobutyl ketone (MIBK) and isopropanol (IPA) in a 1:3 ratio. The MIBK was diluted in order to obtain well-defined profiles. The sample was immersed in this solution and agitated manually for 90 s: a pure IPA solution has been used for 1 min to stop the development of the resist. Then, the pattern was transferred to the thin Si film by reactive ion etching (RIE), using a CF_4 plasma, 50 WRF power and a total gas pressure of 5.4 mTorr. Finally, the resist was removed using acetone. The sample surface was then exposed to O_2 plasma in order to remove the residual resist. Additional chemical cleaning has been performed in N_2 atmosphere before dewetting, by dipping the sample in a 5% HF solution for 20 s. EBL and RIE were performed following a well-established procedure schematized in Fig. 1a and the realized structures were characterized by SEM (Fig. 1b) and atomic force microscopy (AFM, Fig. 1c).

The etched patch shapes were simple squares (with side ranging from 500 nm up to 5 μm) and large square patches (5 μm) with additional features etched within them (e.g. holes, dashes, crosses, etc. Fig.1b and 1c). After etching, the samples were immersed in a 4% concentration aqueous HF solution for 5 s in a nitrogen atmosphere to eliminate any native oxide layer formed on top of the SOI. Thus, in the ultra-high vacuum of a molecular beam reactor, the samples have been annealed at high temperature. All the investigated samples were cleaned with an annealing flash at 600 °C for 30 min in order to eliminate any trace of native oxide from the sample surface. Three different samples were annealed with different procedures: Sample A, @740 °C for 15′; sample B, @720 °C for 3 h; sample C, @ 800 °C for 1 h. The samples are characterized by different imaging techniques: AFM, SEM and optical dark-field microscopy (DF). During the DF analysis, the white light was shined with a ~70 degrees angle with respect to the sample surface. The light diffusion was collected by a high numerical aperture (NA = 0.75) 100× magnification objective lens and the images are registered with a colour-C-MOS camera [16]. As the overall collection angle in the NA of the objective lens was smaller than 70 degrees, the direct reflection from the sample was completely rejected and the flat surfaces appeared completely black. Note that the silicon islands were de facto dielectric Mie resonators, thus the collected signal was the resonant scattering from these nano-antennas. This was reflected in the different scattering colours visible in the DF images [11].

3. Results

We first address the effect of the annealing temperature on the final outcome of large and complex, squared patches (Fig. 2). A precise and reproducible ordering of the dewetted structures is only possible using annealing temperature below ~750 °C. In order to highlight this point, we analyse dark-field images of samples B (annealed at 720 °C for 3 h) and sample C (annealed for 800 °C for 1 h).

The bright scattering spots observed in dark field images correspond to individual islands. More precisely, provided that these objects are resonant antennas, different colours are attributed to resonant electromagnetic modes confined in each island [11,12,16]. These spectral resonances reflect their specific size, shape and composition and thus constitute a precise probe of the islands' homogeneity.

For low-temperature annealing we assist to the formation of a few large islands, eventually exhibiting multi-modal size distributions, with a rather good reproducibility of the complex arrangement over several repetitions (the overall patterns are 12 × 12 repetitions of the same patch design, not shown). Differently from the low temperature case, at high temperature the dewetting cannot be controlled and a random organization of many small islands is observed (Fig. 2 b). This feature reminds the typical results obtained via spontaneous dewetting of the same UT-SOI in non-patterned areas (not shown). In these experimental conditions (device thickness 12 nm and low annealing temperature, ~720 °C) the typical length of the underlying dewetting instability leads to isolated islands which are ~800 nm distant one from the other [11]. For the sake of thoroughness, we mention that temperature and patch orientation may influence this value [28].

Based on the previous results we investigate the impact of the overall dewetting time and of the patch size on the stability of simple, squared patches (without additional features etched within the squares) annealed at low temperature (samples A and B, Fig. 3). The relevant features are summarised as follows: 1) for short time annealing the process is not complete and the dewetting front moved of about 300 nm towards the center of the patch; 2) small protrusions start to form at the patch corners; 3) for longer annealing time the protrusion at the corners become more visible accounting for a reduced dewetting speed with respect to flat dewetting fronts along the patch edges; 4) for

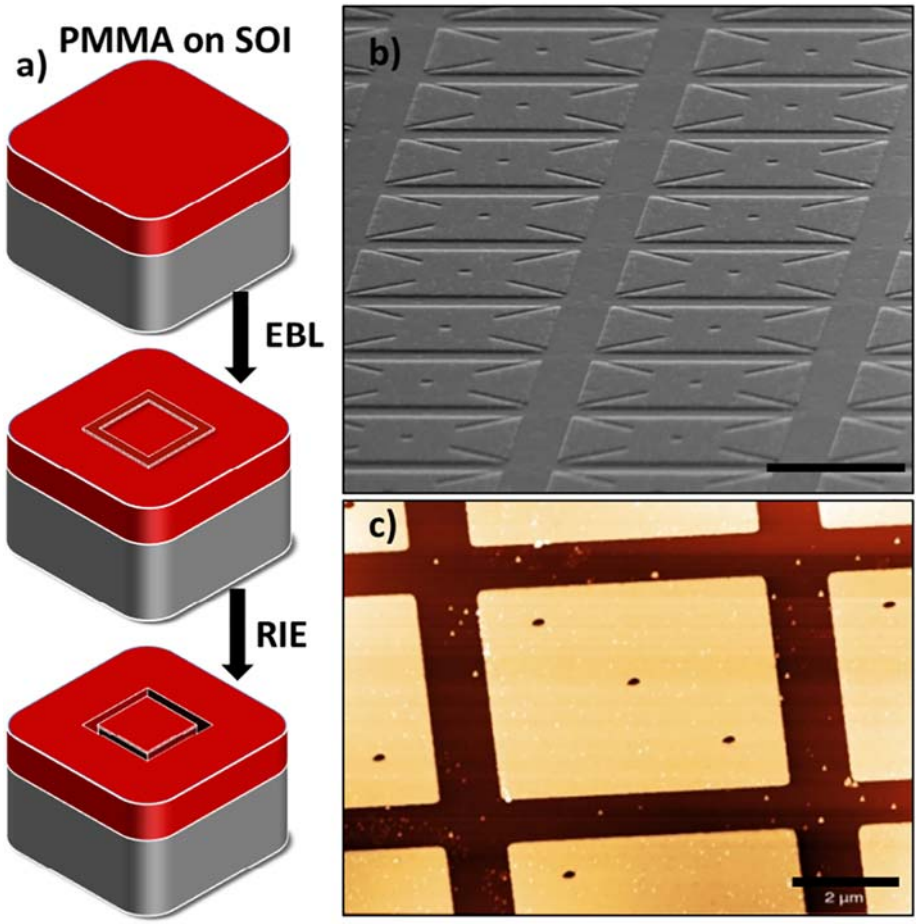

Fig. 1. Experimental methods. a) Schematic sequence of the fabrication steps for patterned squares on thin SOI substrate, where the thicknesses and the size of nanostructures are not in scale. b) SEM image of the complex patterned structures, where some lines and points were introduced into the square patterns to control the dewetting process (ref [16]). c) Typical AFM image of the substrate after the nanofabrication process. In b) and c) the scale bars are 2 µm.

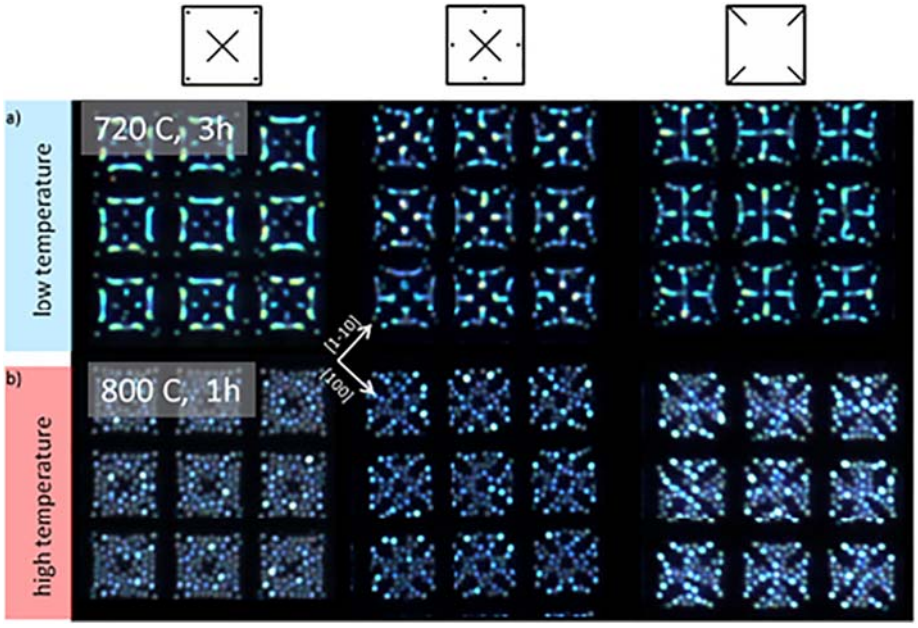

Fig. 2. Role of temperature. a) Optical microscope dark field images of 3 × 3 repetitions of dewetted complex patterns for low temperature annealing (sample B, 720 °C for 3 h). The full pattern includes 12 × 12 identical repetition of the same patch shape (not shown). b) Same as a) for high temperature annealing (sample C, 800 °C for 1 h). The top insets display the initial patch shape etched via e-beam lithography and reactive ion etching prior to annealing.

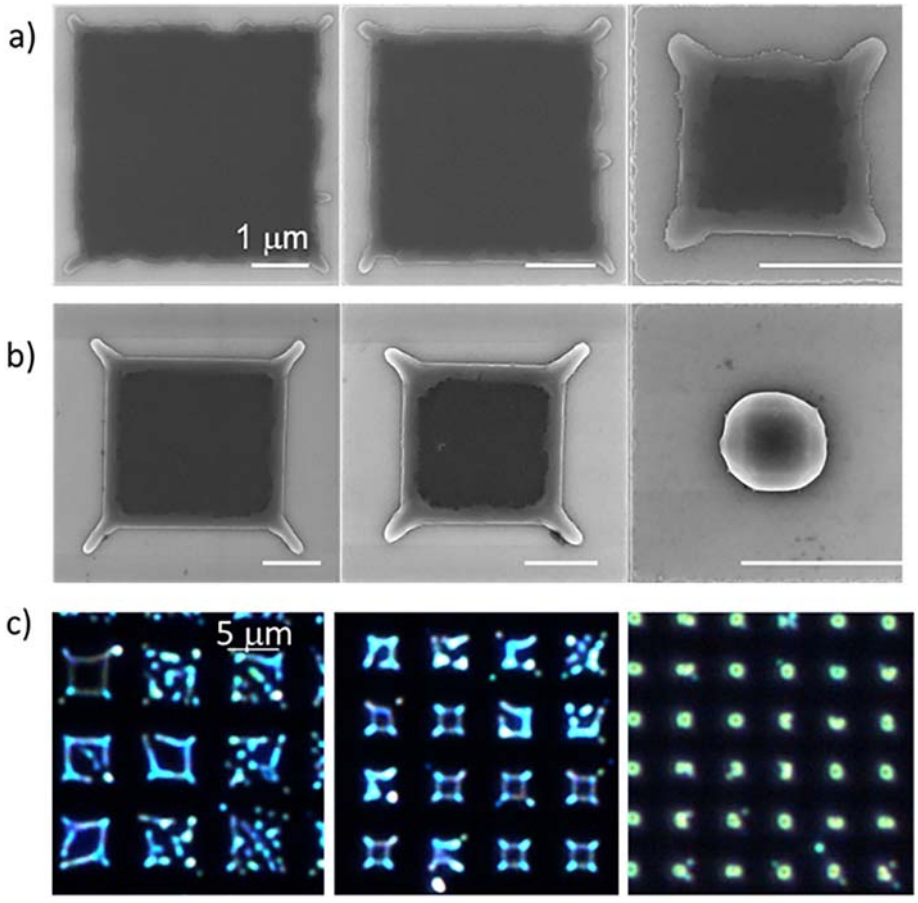

Fig. 3. Short and long-time annealing at low temperature. a) SEM images of simple square patches after dewetting for 15 min at 740 °C (sample A). From the left to the right panel the patch side is reduced from 5 to 1.7 μm. The scale bar corresponds to 1 μm. b) Same as a) for long time annealing, 3 h at 720 °C (sample B). c) Optical microscope, dark field images of sample B for longer annealing time. The four panels display a few repetitions of simple squared patches having size corresponding to those shown in b).

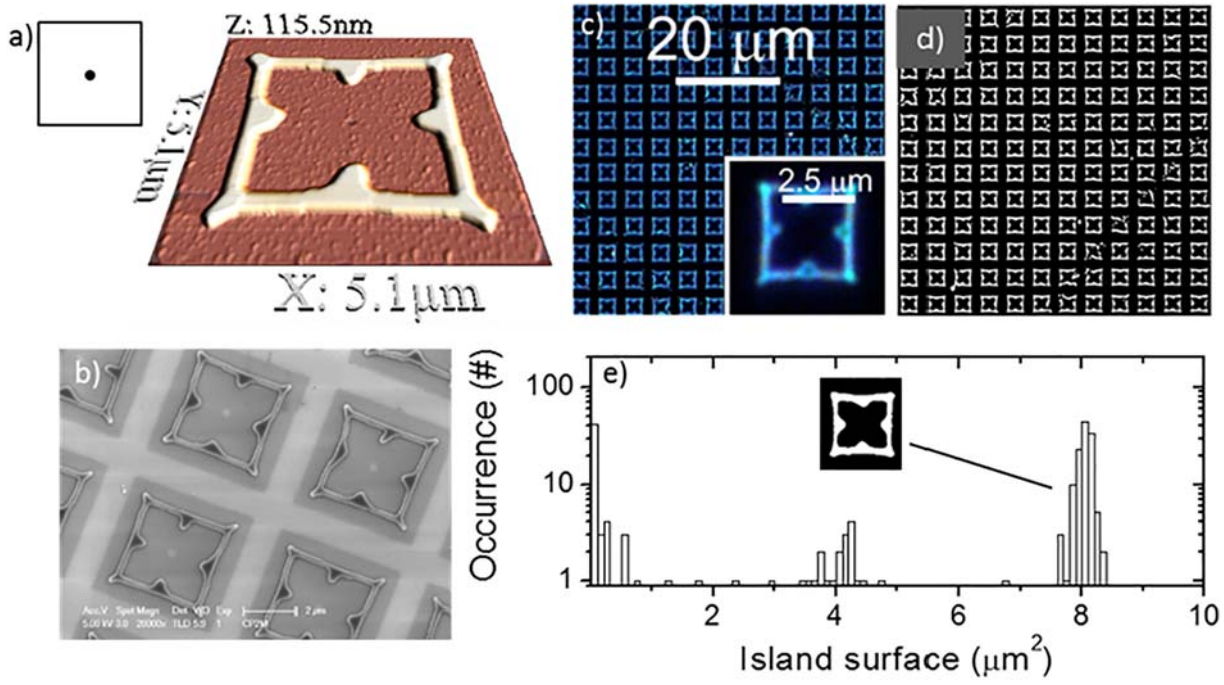

Fig. 4. Dewetting of large complex patches. a) Prospective view of a dewetted, square patch having 5 μm side and a hole milled at its center. The top left inset displays the shape of the etched patch via e-beam lithography and reactive ion etching. b) SEM image of 4 repetitions of the patch shown in a). c) Optical microscope dark field image of the full array (12 × 12 repetitions) of the patch shown in a) and b). The bottom-right inset shows a blow-up of an individual patch. d) Binary image obtained from the image in c). e) Statistic of patch size obtained from the image shown in d). The vertical axis is in logarithmic scale. The inset shows a blow-up of an individual patch.

sufficiently small patches (Fig. 3b), right panel), all the mass present in the patch collapses in a large individual island.

However, when looking at several repetitions of the same squared patches for long time annealing with optical dark field microscopy (Fig. 3c), it appears that the final outcome for large patches is not stable (first panels from the left panel in Fig. 3b): in these cases, only a few patches show the feature selected for SEM images, while many of them feature a random nucleation of isolated islands. A deterministic formation of individual islands is possible only for patches smaller than 1.7 μm.

It appears thus, that in order to overcome the intrinsic disorder affecting the stability of solid state dewetting observed for simple, large, square patches a different strategy has to be adopted. Here we follow the same approach used by Ye and co-workers for metallic patches [23,24] and we introduce additional features within large squared patches featuring a side of 5 μm (Fig. 4). Differently from the previous cases of simple squares (Fig. 3) where the UT-SOI is intact at the center of the patch and the rim moves from the edges inward, the presence of a central hole produces additional mass fluxes moving from the center outward (Fig. 4a) and b)). The presence of the hole has a dramatic impact on the shape of the dewetted structure which appears as a complex nano-architecture of islands (4 at the corners and 4 at the center of each side of the square) connected by wires. The overall height of the structure is ~100 nm while the diameter of the wires is about 200 nm.

Remarkably, when looking at the full array of the dewetted patches, we observe that the complex and almost identical shapes are precisely reproduced over many repetitions (Fig. 4c)). In order to quantify the stability of the outcome and its disorder we evaluate the area of each patch transforming the dark field image in a binary image (0 = absence of an island, 1 = presence of an island, Fig. 4d)) and measuring the statistical distribution of the islands' extension (Fig. 4e)). From this statistical analysis emerges that most of the patches feature an average size of about 8 μm^2 with a standard deviation of ~0.1 μm^2 (corresponding to a size fluctuation of a few percentage). Additional characterizations performed with other imaging techniques (e.g. SEM) confirm that the fluctuations of the sharp features composing the complex nanoarchitectures fluctuate of a few percentages (not shown). For the sake of thoroughness, we observe that some event is visible in the size distribution at ~4 μm^2. These events occur at about the half of the full patch size and thus, are attributed to patches broken into two separate parts. Finally, a few, isolated, small islands are present below 1 μm^2 area, accounting for some residual randomness in the system.

4. Discussion

The features of the dewetting process illustrated in Figs. 2, 3 and 4 are explained by taking into account the surface-diffusion limited-kinetics mechanism at the basis of solid-state dewetting of crystalline thin films. The local curvature of the surface (eventually modified by the artificial introduction of edges, holes, trenches etc.) determines a gradient in the chemical potential which is the driving force for (anisotropic) mass transport on the film surface. During this process, mass is accumulated in a thick receding rim formed at the edges of the patches which in turn becomes unstable under the action of additional instabilities (fingering, rim pinch-off, bulging, faceting, etc.). Thus, for small enough patches (smaller or of the order of the intrinsic wavelength of the underlying instability, ~800 nm in the present case) all the receding rims collapse in a central, large island. More precisely, for simple squared patches the presence of corners locally increases the curvature further modifying the behaviour of mass transport with respect to simple, flat, receding rims (e.g. the long protrusion at the patch edges visible in Fig. 3a) and b)).

The presence of additional etched features within the square patch produce further mass fluxes (e.g. from the central hole outward, as in Fig. 4) which can be engineered to control the final morphologies. Remarkably, for patches featuring a side of 5 μm (about 6 times larger than the "natural" wavelength of the instability) the outward-moving rims stabilises the inward-moving ones preventing their uncontrolled break-up in small islands (as shown in Fig. 3c for large squares). All these features are thoroughly described in reference and in the videos in [16].

The results shown in Fig. 2 demonstrate that only in a low-temperature regime a good control of the dewetting fronts can be obtained, avoiding their separation in isolated islands. This is interpreted as a hierarchical onset of different instabilities in silicon: after rim formation at the patch edges, the large surface anisotropy of the underlying crystal promotes the formation of facets rendering the rim unstable and breaking it in isolated islands (Fig. 2a). However, for lower annealing temperature, a partial control of the rim evolution can be recovered and a coherent break-up in organized oligomers is observed (Fig. 2b), suggesting that the instability of the rim occurs at later times. Thus, lowering the annealing temperature is one of the key parameters for controlling the dewetting fronts.

In spite of the better control achieved for low annealing temperature, simple squares provide a deterministic result only for small patches (Fig. 3b) and c)): for stable dewetting fronts the rim can evolve for about 1 μm without the onset of any additional perturbation providing a good control of the final outcome in small patches (side shorter than ~1.7 μm). Provided that the underlying instability for spontaneous dewetting in non-patterned areas, is about 800 nm, large patches exceeding several times this value, undergo a chaotic behaviour and break-up in many isolated islands. Thus, adopting modified patch geometry we observe a highly reproducible and precise result (Fig. 4): additional features introduced in the initial pattern (such as the dashes and holes of Fig. 1 or the central hole of Fig. 4), produce further mass fluxes which can be designed to determine the final dewetted morphologies.

These results demonstrate that solid state dewetting can be exploited to produce mono-crystalline objects with atomically smooth surfaces, free of defects, arranged in large arrays of identical replicas and quantifies the sizes and the temperature that should be adopted in the process. This is relevant in view of the exploitation of this method for electronic and photonic components. We also stress that, differently from conventional top-down methods, the size of the dewetted structures can be reduced to extremely small values by reducing the initial UT-SOI thickness, in principle overcoming the resolution limits of e-beam lithography. Finally, further tuning of the islands shape can be obtained via Ge alloying before or after dewetting [13,14,29,30,31].

5. Conclusion

In conclusion, we demonstrated a method based on e-beam lithography and reactive ion etching for controlling the solid state dewetting of ultra-thin silicon films on insulator. Working at lower temperature and with a proper pattern, the surface diffusion mechanism in the UT-SOI film can be controlled. In the light of the experimental results and recent simulations based on the continuum modelling of surface diffusion by means of a phase field model [16], it is known that a spontaneous phenomenon can be efficiently engineered for the formation of monocrystalline nano-architectures with high reproducibility and precision. In spite of the tendency of thin silicon films to rapidly break into islands upon annealing, our findings clearly demonstrate that the common underlying mechanism at play, surface diffusion limited kinetics, provides qualitatively similar results for the two cases. These results are relevant for applications in photonics for the fabrication of dielectric meta-surfaces as well as waveguides, diffraction gratings, interferometers and much more. Nevertheless, the relevance of silicon for microelectronics makes our method a strategic tool for the implementation of complex electrically-isolated nano-circuits.

Acknowledgements

We acknowledge the support of the Alexander von Humboldt Foundation; the projects PHC MAGHREB (no. 32595SL), EMMAG-Erasmus

Mundus Maghreb & Egypt; the Nanotecmat Platform of the IM2NP Institute of Marseilles and the CP2M microscopy center of the Aix-Marseilles University for the availability of the tools and the equipment needed for this study. We thank Dominique Chatain for the discussions about the experimental; Valeria Mondiali for the useful discussions on electron beam lithography and nano-imprinting fabrications.

The authors declare that they have no competing interests or conflicts of interests.

Data and materials availability: All data needed to evaluate the conclusions in the paper are present in the paper. Additional data related to this paper may be requested from the corresponding authors.

References

[1] J.-P. Colinge, Silicon-on-Insulator Technology: Materials to VLSI: Materials to Vlsi, Springer Science & Business Media, 2004.
[2] A.M. Cazabat, et al., Fingering instability of thin spreading films driven by temperature gradients, Nature 346 (6287) (1990) 824.
[3] Carl V. Thompson, Solid-state dewetting of thin films, Annu. Rev. Mater. Res. 42 (2012) 399–434.
[4] Olivier Pierre-Louis, Anna Chame, Yukio Saito, Dewetting of ultrathin solid films, Phys. Rev. Lett. 103 (19) (2009) 195501.
[5] F. Cheynis, E. Bussmann, F. Leroy, T. Passanante, P. Müller, Dewetting dynamics of silicon-on-insulator thin films, Phys. Rev. B 84 (24) (2011) 245439.
[6] William W. Mullins, Theory of thermal grooving, J. Appl. Phys. 28 (3) (1957) 333–339.
[7] R.V. Zucker, G.H. Kim, W.C. Carter, C.V. Thompson, A model for solid-state dewetting of a fully-faceted thin film, C. R. Phys. 14 (7) (2013) 564–577.
[8] M. Dufay, O. Pierre-Louis, Anisotropy and coarsening in the instability of solid dewetting fronts, Phys. Rev. Lett. 106 (10) (2011) 105506.
[9] F. Leroy, F. Cheynis, T. Passanante, P. Müller, Dynamics, anisotropy, and stability of silicon-on-insulator dewetting fronts, Phys. Rev. B 85 (19) (2012) 195414.
[10] D.T. Danielson, PhD Thesis Anisotropic Dewetting in Ultra-Thin Single-Crystal Silicon-On-Insulator Films. , Massachusetts Institute of Technology, 2008.
[11] Marco Abbarchi, Meher Naffouti, Benjamin Vial, Abdelmalek Benkouider, Laurent Lermusiaux, Luc Favre, Antoine Ronda, Sébastien Bidault, Isabelle Berbezier, Nicolas Bonod, Wafer scale formation of monocrystalline silicon-based Mie resonators via silicon-on-insulator dewetting, ACS Nano 8 (11) (2014) 11181–11190.
[12] Meher Naffouti, Thomas David, Abdelmalek Benkouider, Luc Favre, Antoine Ronda, Isabelle Berbezier, Sebastien Bidault, Nicolas Bonod, Marco Abbarchi, Fabrication of poly-crystalline Si-based Mie resonators via amorphous Si on SiO2 dewetting, Nano 8 (5) (2016) 2844–2849.
[13] M. Aouassa, I. Berbezier, L. Favre, A. Ronda, M. Bollani, R. Sordan, A. Delobbe, P. Sudraud, Design of free patterns of nanocrystals with ad hoc features via templated dewetting, Appl. Phys. Lett. 101 (2012), 013117. .
[14] I. Berbezier, M. Aouassa, A. Ronda, L. Favre, M. Bollani, R. Sordan, A. Delobbe, P. Sudraud, Ordered arrays of Si and Ge nanocrystals via dewetting of pre-patterned thin films, J. Appl. Phys. 113 (6) (2013), 064908. .
[15] Meher Naffouti, Thomas David, Abdelmalek Benkouider, Luc Favre, Anne Delobbe, Antoine Ronda, Isabelle Berbezier, Marco Abbarchi, Templated solid-state dewetting of thin silicon films, Small 12 (44) (2016) 6115–6123.
[16] M. Naffouti, R. Backofen, M. Salvalaglio, T. Bottein, M. Lodari, A. Voigt, T. David, A. Benkouider, I. Fraj, L. Favre, A. Ronda, I. Berbezier, D. Grosso, M. Abbarchi, M. Bollani, Complex dewetting scenarios of ultra-thin silicon films for large-scale nano-architectures, Sci. Adv. 3 (11) (2017), eaao1472. .
[17] D.J. Srolovitz, S.A. Safran, Capillary instabilities in thin films. I. Energetics, J. Appl. Phys. 60 (1) (1986) 247–254.
[18] D.J. Srolovitz, S.A. Safran, Capillary instabilities in thin films. II. Kinetics, J. Appl. Phys. 60 (1) (1986) 255–260.
[19] E. Jiran, C.V. Thompson, Capillary instabilities in thin films, J. Electron. Mater. 19 (11) (1990) 1153–1160.
[20] Y. Ishikawa, M. Kumezawa, R. Nuryadi, M. Tabe, Appl. Surf. Sci. 190 (2002) 11.
[21] Y. Ishikawa, Y. Imai, H. Ikeda, M. Tabe, Appl. Phys. Lett. 83 (2003) 3162.
[22] M. Trautmann, F. Cheynis, F. Leroy, S. Curiotto, O. Pierre-Louis, P. Müller, Appl. Phys. Lett. 110 (263105) (2017).
[23] J. Ye, C.V. Thompson, Templated solid-state dewetting to controllably produce complex patterns, Adv. Mater. 23 (13) (2011) 1567–1571.
[24] Jongpil Ye, Carl V. Thompson, Regular pattern formation through the retraction and pinch-off of edges during solid-state dewetting of patterned single crystal films, Phys. Rev. B 82 (19) (2010) 193408.
[25] Jongpil Ye, Fabrication of ordered arrays of micro-and nanoscale features with control over their shape and size via templated solid-state dewetting, Sci. Rep. 5 (2015).
[26] F. Leroy, F. Cheynis, Y. Almadori, S. Curiotto, M. Trautmann, J.C. Barbe, P. Müller, Surf. Sci. Rep. 71 (2016) 391.
[27] B. Li, J. Lowengrub, A. Rätz, A. Voigt, Commun. Comput. Phys. 6 (433) (2009).
[28] B. Legrand, V. Agache, T. Mélin, J.P. Nys, V. Senez, D. Stiévenard, J. Appl. Phys. 91 (2002) 106.
[29] E. Sutter, P. Sutter, Assembly of Ge nanocrystals on SiO_2 via a stress-induced dewetting process, Nanotechnology 17 (15) (2006) 3724.
[30] P.P. Zhang, B. Yang, P.P. Rugheimer, M.M. Roberts, D.E. Savage, Feng Liu, M.G. Lagally, Influence of germanium on thermal dewetting and agglomeration of the silicon template layer in thin silicon-on-insulator, J. Phys. D. Appl. Phys. 42 (17) (2009), 175309. .
[31] Meher Naffouti, Thomas David, Abdelmalek Benkouider, Luc Favre, Martiane Cabie, Antoine Ronda, Isabelle Berbezier, Marco Abbarchi, Fabrication of core–shell nanostructures via silicon on insulator dewetting and germanium condensation: towards a strain tuning method for SiGe-based heterostructures in a three-dimensional geometry, Nanotechnology 27 (30) (2016) 305602.